

# Geometric Information Decomposition for Weighted Empirical Measures on the Sphere

Kisung You  
Baruch College

## Abstract

We study directional uncertainty when the data already represent a weighted probability measure on the unit sphere, as in importance samples, quadrature rules, or attention-weighted embeddings. A standard approach fits a von Mises–Fisher distribution and reports its concentration or entropy. This is principled but incomplete because vMF uses only mean-direction information and can miss antipodal, axial, girdle-like, or multimodal structure. We introduce the geometric information decomposition (GID), which fits a nested sequence of maximum-entropy projections using spherical features and reports the entropy gap added at each level. The first gap recovers vMF information, the second captures Fisher–Bingham/Bingham-type anisotropy, and later gaps capture finer angular structure. We prove invariance, consistency, asymptotic normality away from zero gaps, and a quadratic-form null calibration for deciding whether a new level carries information. Experiments on circular and spherical examples, calibration studies, and a query-weighted digit projection show when vMF uncertainty suffices and when higher-order gaps reveal hidden structure.

## 1 INTRODUCTION

We begin with a probability measure on the  $(d - 1)$ -dimensional sphere  $S^{d-1}$  embedded in  $\mathbb{R}^d$  represented by weighted support points,

$$\hat{P}_w = \sum_{i=1}^n w_i \delta_{x_i}, \quad x_i \in S^{d-1}, \quad w_i \geq 0, \quad \sum_{i=1}^n w_i = 1. \quad (1)$$

The weights determine integration under the represented law. Uniform weights  $w_i = 1/n$  recover the

usual empirical distribution, while nonuniform weights appear in posterior particles, importance samples, quadrature rules, reliability- or survey-weighted directions, and attention-weighted normalized embeddings. Given (1), the natural question is to summarize the geometric variability of the probability law on  $S^{d-1}$ .

A standard model-based summary fits a von Mises–Fisher (vMF) distribution (Fisher, 1953). With

$$\hat{r} = \sum_{i=1}^n w_i x_i, \quad \hat{R} = \|\hat{r}\|,$$

the vMF fit converts  $\hat{R}$  into a concentration  $\hat{\kappa}$  and, if desired, into fitted entropy or Kullback–Leibler (KL) divergence from uniformity. This is appealing because  $\hat{\kappa}$  is a single interpretable number. Large values indicate high concentration around one direction, while  $\hat{\kappa} \approx 0$  means the fitted vMF law is nearly uniform.

This first-order viewpoint can fail in simple cases. If  $P$  places equal mass near  $\mu$  and  $-\mu$ , then  $\mathbb{E}_P[X] \approx 0$ , so the fitted vMF model is nearly uniform even though  $P$  is sharply concentrated around an axis. If  $P$  is concentrated near an equator, the mean direction again vanishes although the distribution has strong girdle structure. If  $P$  has several separated modes arranged symmetrically, low-order moments may cancel while the distribution remains far from uniform. In all of these cases, reporting only  $\hat{\kappa}$  confuses absence of preferred mean direction with high uncertainty.

We replace the single first-moment fit by nested maximum-entropy projections. Let  $\mathcal{V}_L$  be the spherical feature space used at level  $L$ , for example the span of spherical harmonics up to degree  $L$ . Define  $p_L^P$  as the maximum-entropy density on  $S^{d-1}$  whose  $\mathcal{V}_L$  moments agree with those of  $P$ . Thus  $p_L^P$  is the least structured density that preserves the geometric information visible at level  $L$ . Its entropy deficit from uniformity,

$$D_L(P) = \text{KL}(p_L^P \sigma \parallel \sigma),$$

where  $\sigma$  is normalized surface measure, is the non-uniform information explained by all features up to

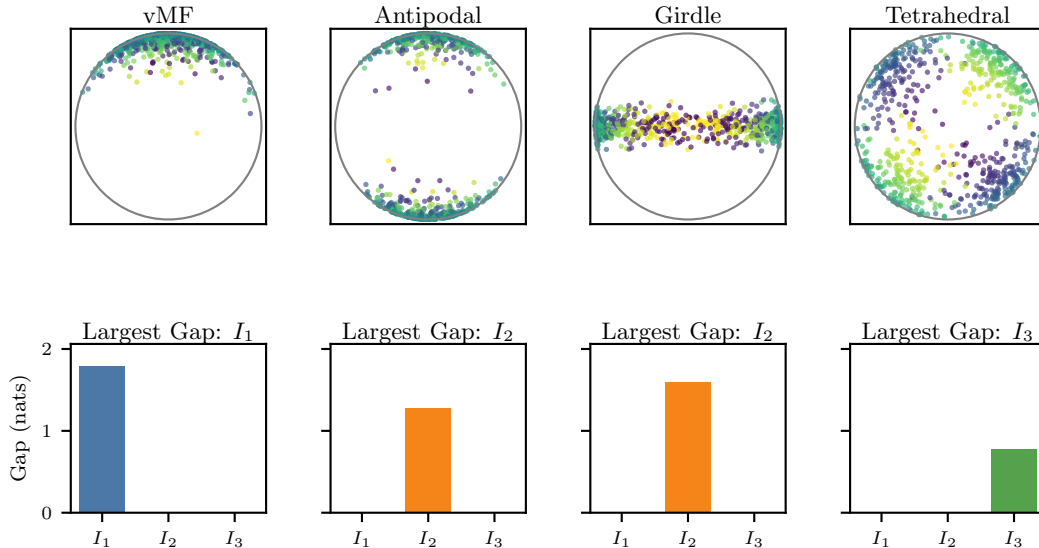


Figure 1: Geometry-to-information fingerprint on  $S^2$ . The top row shows representative point clouds under an orthographic projection and the bottom row reports the first three information gaps from the harmonic maximum-entropy hierarchy. vMF structure is first-order, antipodal and girdle structure are second-order, and the tetrahedral example first appears at a higher harmonic level.

level  $L$ . The increment  $I_L(P) = D_L(P) - D_{L-1}(P)$  is the additional information explained by level  $L$  features. We call the profile vector

$$(I_1(P), I_2(P), \dots, I_L(P))$$

the *geometric information decomposition* (GID). Level 1 recovers vMF mean-direction information and level 2 captures Fisher–Bingham/Bingham-type axiality, antipodal structure, ellipticity, and girdles. Higher harmonic levels capture finer angular structure, including multimodality. The full harmonic hierarchy is a low- and moderate-dimensional directional method. For large-scale data where full degree-two and higher spaces are too large to use, one can use structured or projected features, which is discussed in Section 7.

Although the motivation and examples are spherical, the same construction has a compact-manifold formulation. In the notation below,  $\nu$  denotes normalized Riemannian volume, with  $\nu = \sigma$  on the sphere. The structural identity

$$I_L(P) = \text{KL}(p_L^P \nu \parallel p_{L-1}^P \nu)$$

is a specialization of the information-geometric Pythagorean and hierarchical KL decompositions, not a new identity in isolation. Our contribution is to use this hierarchy as a statistically estimable uncertainty decomposition for measures represented as in (1).

**Contributions.** We define a sphere-first GID for empirical probability measures of the form (1), treating

vMF concentration as the first entropy gap rather than as a complete uncertainty summary. Building on the classical hierarchical KL decomposition, we specialize nested maximum-entropy projections to spherical feature spaces and establish basis and rotation invariance, consistency, first-order normal limits away from zero gaps, and a second-order quadratic-form calibration for testing whether a new level carries information. We also give concrete directional interpretations of the low-order gaps, clarify the computational limits of full harmonic fitting beyond moderate dimension, and propose structured or projected feature spaces for embedding-scale settings. Experiments on  $S^1$  and  $S^2$ , a finite-sample null-calibration study, and a query-weighted digit example after spherical projection show when vMF uncertainty is adequate and when higher-order gaps reveal hidden structure. Code to reproduce experimental results and figures can be found at <https://github.com/kisungyou/GeoInfoDec>.

## 2 RELATED WORK

**Maximum entropy and information geometry.** The maximum-entropy principle (Jaynes, 1957) selects the least informative distribution satisfying prescribed constraints, and moment-constrained maximum entropy is dual to likelihood fitting in exponential families. Its KL geometry is classical. Csiszar (1975) developed information projection, while Amari et al. (2007) and Amari (2001) studied the Pythagorean and hier-

archical decompositions underlying nested exponential families. Our KL-gap identity is a specialization of this information-geometric lineage. The contribution is to use the hierarchy as an uncertainty profile for weighted empirical measures on the sphere, with directional interpretation, estimation, and null calibration. Boundary and existence issues follow standard exponential-family theory (Brown, 1986; Csiszar and Matus, 2003).

**Directional distributions.** Directional statistics provides the low-order models that motivate our hierarchy (Mardia and Jupp, 2000). The vMF distribution is the canonical first-order model on the sphere and is widely used for normalized observations and spherical clustering (Fisher, 1953; Banerjee et al., 2005). Second-order directional structure is modeled by Bingham, Fisher–Bingham, Kent, and related families. In particular, Beran (1979) studied exponential models including Fisher/vMF and Bingham cases, and Kent (1982) introduced the Fisher–Bingham distribution on  $S^2$  as a spherical analogue of a general bivariate normal distribution. We do not propose these as unrelated model choices. Instead, we arrange them as successive maximum-entropy projections whose entropy gaps quantify mean-direction, axial/girdle, and higher-order structure.

**Higher-order models, computation, and diagnostics.** For richer angular structure, harmonic exponential families on compact homogeneous manifolds provide a flexible likelihood framework based on harmonic analysis (Cohen and Welling, 2015). This is close to our high-order spherical construction, but our focus is interpretability of the gap profile rather than flexible density estimation alone. Computationally, second-order spherical exponential families require nontrivial normalizing constants; saddlepoint approximations for Bingham-type models are an important practical tool (Kume and Wood, 2005). Finally, goodness-of-fit and uniformity testing on spheres and compact manifolds motivate the residual diagnostics used alongside the gaps (Jupp, 2008; García-Portugués and Verdebout, 2018). A low-order entropy summary is useful only when the corresponding fitted projection adequately represents the observed measure.

### 3 SETUP

Let  $M$  be a connected compact Riemannian manifold without boundary, and let  $\nu$  denote normalized Riemannian volume, so  $\nu(M) = 1$ . All densities are taken with respect to  $\nu$ . Compactness is not essential for every definition below, but it gives a canonical uniform reference distribution and avoids integrability compli-

cations. We write  $\mathcal{P}(M)$  for the set of Borel probability measures on  $M$ .

Denote by

$$\mathcal{V}_0 \subset \mathcal{V}_1 \subset \dots \subset \mathcal{V}_L \subset L_0^2(M, \nu)$$

the nested finite-dimensional spaces of continuous, mean-zero functions, where  $L_0^2$  denotes functions with zero  $\nu$ -mean. The zero level  $\mathcal{V}_0 = \{0\}$  corresponds to the uniform distribution. Let  $q_L = \dim(\mathcal{V}_L)$  and let  $\phi_L : M \rightarrow \mathbb{R}^{q_L}$  be a basis vector for  $\mathcal{V}_L$ . For  $P \in \mathcal{P}(M)$ , define the moment vector

$$m_L(P) = \int_M \phi_L(x) dP(x).$$

For (1), the plug-in moment is

$$\hat{m}_L = m_L(\hat{P}_w) = \sum_{i=1}^n w_i \phi_L(x_i).$$

This is the default empirical integration rule throughout. Unless stated otherwise, all empirical moments, likelihoods, estimates, and calibrations are computed by integration against  $\hat{P}_w$ , so we do not repeat the qualifier “weighted” below.

The feasible moment body is

$$\mathcal{M}_L = \text{conv}\{\phi_L(x) : x \in M\} \subset \mathbb{R}^{q_L}.$$

A moment vector on the boundary of  $\mathcal{M}_L$  can force a degenerate solution. Throughout the main statements, we assume that the relevant moment vector lies in  $\text{ri}(\mathcal{M}_L)$ , the relative interior of  $\mathcal{M}_L$ .

For  $m \in \text{ri}(\mathcal{M}_L)$ , define the maximum-entropy density

$$p_{L,m} = \arg \max_p - \int_M p \log p d\nu$$

$$\text{s.t. } \int_M p d\nu = 1, \quad \int_M \phi_L p d\nu = m.$$

When  $m = m_L(P)$ , we write  $p_L^P = p_{L,m_L(P)}$ . When  $m = \hat{m}_L$ , we write  $\hat{p}_L = p_{L,\hat{m}_L}$ .

The dual log-partition function is

$$\psi_L(\lambda) = \log \int_M \exp\{\lambda^\top \phi_L(x)\} d\nu(x).$$

The maximum-entropy solution has exponential-family form

$$p_{L,m}(x) = \exp\{\lambda_L(m)^\top \phi_L(x) - \psi_L(\lambda_L(m))\},$$

where  $\lambda_L(m)$  solves

$$\nabla \psi_L(\lambda_L(m)) = m.$$

Equivalently,  $\lambda_L(m)$  maximizes

$$\lambda^\top m - \psi_L(\lambda).$$

Thus the plug-in estimator  $\hat{p}_L$  is the sample-weighted likelihood fit

$$\begin{aligned} \hat{\lambda}_L &= \arg \max_{\lambda \in \mathbb{R}^{q_L}} \{\lambda^\top \hat{m}_L - \psi_L(\lambda)\} \\ &= \arg \max_{\lambda} \sum_{i=1}^n w_i \log p_{\lambda,L}(x_i). \end{aligned}$$

## 4 GEOMETRIC INFORMATION DECOMPOSITION

### 4.1 Entropy Deficits and Effective Uncertainty

Because  $\nu$  is normalized, the uniform density  $p \equiv 1$  has zero entropy, and every density has nonpositive entropy:

$$h(p) = - \int_M p \log p \, d\nu \leq 0.$$

We define the level- $L$  entropy deficit from uniformity by

$$D_L(P) = \text{KL}(p_L^P \nu \parallel \nu) = \int_M p_L^P \log p_L^P \, d\nu.$$

The corresponding effective uncertainty is

$$U_L(P) = \exp\{-D_L(P)\} \in (0, 1].$$

Thus  $U_L(P) = 1$  if the matched features carry no non-uniform information, while smaller values indicate greater concentration or structure explained by the features.

The level- $L$  information gap is

$$I_L(P) = D_L(P) - D_{L-1}(P), \quad L \geq 1.$$

The empirical versions are

$$\hat{D}_L = D_L(\hat{P}_w), \quad \hat{U}_L = \exp\{-\hat{D}_L\}, \quad \hat{I}_L = \hat{D}_L - \hat{D}_{L-1}. \quad (2)$$

### 4.2 Main Structural Properties

The following theorem is the structural identity behind the decomposition. It is the nested maximum-entropy specialization of classical information-geometric Pythagorean identities (Csiszar, 1975; Amari, 2001; Amari et al., 2007). The novelty here is its sphere-specific use as an uncertainty diagnostic for (1).

**Theorem 1** (Monotonicity and KL-gap identity). *Assume that  $m_L(P) \in \text{ri}(\mathcal{M}_L)$  for  $L = 0, 1, \dots, L_{\max}$  and that the feature spaces are nested. Then*

$$0 = D_0(P) \leq D_1(P) \leq \dots \leq D_{L_{\max}}(P).$$

Moreover, for each  $L \geq 1$ ,

$$I_L(P) = D_L(P) - D_{L-1}(P) = \text{KL}(p_L^P \nu \parallel p_{L-1}^P \nu). \quad (3)$$

Consequently,

$$D_L(P) = \sum_{\ell=1}^L I_\ell(P). \quad (4)$$

The identity (3) says that the incremental entropy deficit from adding level- $L$  features is exactly the information distance between the refined and coarser maximum-entropy projections. This justifies calling  $I_L(P)$  the level- $L$  information gap.

**Theorem 2** (Basis invariance). *Let  $\tilde{\phi}_L = T\phi_L$  for an invertible matrix  $T$ . Then the maximum-entropy density  $p_L^P$ , entropy deficit  $D_L(P)$ , effective uncertainty  $U_L(P)$ , and increments  $I_L(P)$  are unchanged.*

Basis invariance matters because the feature spaces, not the coordinates used to represent them, are the geometric objects.

**Theorem 3** (Isometry invariance). *Let  $\Gamma$  be a group of isometries of  $M$ . Suppose each feature space  $\mathcal{V}_L$  is invariant under composition with  $g \in \Gamma$ , i.e.  $f \in \mathcal{V}_L$  implies  $f \circ g^{-1} \in \mathcal{V}_L$ . Then for every  $P \in \mathcal{P}(M)$  and  $g \in \Gamma$ ,*

$$\begin{aligned} D_L(g\#P) &= D_L(P), \\ U_L(g\#P) &= U_L(P), \\ I_L(g\#P) &= I_L(P). \end{aligned}$$

On the sphere, taking  $\mathcal{V}_L$  to be complete spherical harmonic degree spaces gives rotation invariance. Hence the decomposition is a property of the distribution's geometry, not of the coordinate system.

## 5 ESTIMATION THEORY

The construction defines population functionals  $D_L(P)$  and  $I_L(P)$ , estimated by the plug-ins (2). The method has two compatible uses: a descriptive one where  $\hat{P}_w$  is itself the object of interest, and an inferential one where  $\hat{P}_w$  is a random representation of an underlying  $P$ . The calibration and testing results require the latter: deterministic quadrature supports consistency but does not by itself define sampling  $p$ -values. Because the assumptions are stated as moment convergence, they cover the unweighted empirical distribution, nonuniform deterministic weights, importance

samples, and quadrature approximations alike, whenever the corresponding moment law of large numbers or central limit theorem holds.

**Assumption 4** (Interior and identifiability). For the levels under consideration,  $m_L(P) \in \text{ri}(\mathcal{M}_L)$ . The exponential family generated by  $\phi_L$  is minimal after quotienting out linear dependencies that are constant  $\nu$ -almost surely.

**Assumption 5** (Moment convergence). For each fixed  $L$ ,

$$\widehat{m}_L = \sum_{i=1}^n w_i \phi_L(x_i) \xrightarrow{P} m_L(P).$$

**Theorem 6** (Consistency). Under Assumptions 4 and 5, for each fixed  $L$ ,

$$\widehat{\lambda}_L \xrightarrow{P} \lambda_L(P), \quad \widehat{D}_L \xrightarrow{P} D_L(P), \quad \widehat{I}_L \xrightarrow{P} I_L(P).$$

For asymptotic normality, suppose the plug-in moments satisfy a CLT:

$$a_n \{\widehat{m}_L - m_L(P)\} \Rightarrow N(0, \Sigma_L), \quad (5)$$

for some  $a_n \rightarrow \infty$ . In the common independent deterministic-weight case with  $X_i \sim P$ , one has  $a_n = (\sum_i w_i^2)^{-1/2}$  under a Lindeberg condition such as

$$\frac{\max_i w_i}{(\sum_j w_j^2)^{1/2}} \rightarrow 0.$$

The quantity  $(\sum_i w_i^2)^{-1}$  is the usual effective sample size for the representation, but the theorem itself only requires (5).

Let

$$D_L(m) = \sup_{\lambda} \{\lambda^\top m - \psi_L(\lambda)\}.$$

Then  $D_L(P) = D_L(m_L(P))$  and

$$\nabla_m D_L(m) = \lambda_L(m).$$

**Theorem 7** (Delta-method asymptotics away from zero gaps). Assume 4 and the moment CLT (5). The following statements hold on the event  $\{\widehat{m}_L \in \text{ri}(\mathcal{M}_L)\}$ , which has probability tending to one. Then

$$a_n (\widehat{D}_L - D_L(P)) \Rightarrow N(0, \lambda_L(P)^\top \Sigma_L \lambda_L(P)).$$

For the increment  $I_L = D_L - D_{L-1}$ , write  $\Pi_{L-1}$  for the coordinate projection from level  $L$  moments to level  $L-1$  moments, and define

$$\gamma_L = \lambda_L(P) - \Pi_{L-1}^\top \lambda_{L-1}(P),$$

where  $\lambda_{L-1}$  is embedded in the level- $L$  coordinate system. Then

$$a_n (\widehat{I}_L - I_L(P)) \Rightarrow N(0, \gamma_L^\top \Sigma_L \gamma_L). \quad (6)$$

Theorem 7 is an alternative-regime statement. It is not a valid calibration for testing whether an information gap is zero, because then the first derivative of  $I_L$  vanishes. The correct local calibration is second order.

**Theorem 8** (Second-order null calibration). Write the level- $L$  feature vector as  $\phi_L = (u, v)$ , where  $u$  spans  $\mathcal{V}_{L-1}$  and  $v$  spans the added coordinates, so  $q = q_L - q_{L-1}$ . Suppose  $I_L(P) = 0$ , equivalently  $p_L^P = p_{L-1}^P$ , and let  $\theta_0 = (\alpha_0, 0)$  be the corresponding level- $L$  natural parameter. Define

$$\mathcal{J}_0 = \text{Var}_{\theta_0} \{(u(X), v(X))\} = \begin{pmatrix} J_{uu} & J_{uv} \\ J_{vu} & J_{vv} \end{pmatrix}.$$

Under the minimality condition in Assumption 4,  $J_{uu}$  and the Schur complement

$$\mathcal{S} = J_{vv} - J_{vu} J_{uu}^{-1} J_{uv}$$

are positive definite. If

$$a_n \{\widehat{m}_L - m_L(P)\} \Rightarrow Z \sim N(0, \Sigma_L),$$

then

$$a_n^2 \widehat{I}_L \Rightarrow \frac{1}{2} Z^\top \mathcal{N}_0^\top \mathcal{S}^{-1} \mathcal{N}_0 Z, \quad \mathcal{N}_0 = \begin{pmatrix} -J_{vu} J_{uu}^{-1} & I_q \end{pmatrix}. \quad (7)$$

Equivalently, the limit is a weighted sum of independent  $\chi_1^2$  variables, with coefficients given by the eigenvalues of  $\frac{1}{2} \mathcal{S}^{-1/2} \mathcal{N}_0 \Sigma_L \mathcal{N}_0^\top \mathcal{S}^{-1/2}$ . If the representation is correctly specified i.i.d. from the reduced maximum-entropy model with uniform weights, so that  $\Sigma_L = \mathcal{J}_0$  and  $a_n = \sqrt{n}$ , then

$$2a_n^2 \widehat{I}_L \Rightarrow \chi_q^2.$$

If additional inequality constraints, eigenvalue order constraints, or cone constraints are imposed on the new parameters, the corresponding boundary calibration can instead be a chi-bar-square law (Self and Liang, 1987).

Thus standard errors from Theorem 7 are appropriate for nonzero population gaps, while significance of a new level should be assessed using Theorem 8, a sandwich version of the quadratic-form limit, or a bootstrap designed to reproduce the null model.

**Operational null calibration.** Theorem 8 is directly usable by plug-in. First, fit the reduced model and form  $\widehat{\theta}_0 = (\widehat{\alpha}, 0)$  and estimate  $\widehat{\mathcal{J}}_0 = \text{Var}_{\widehat{\theta}_0} \{\phi_L(X)\}$  by quadrature, Monte Carlo, or analytic moments, then partition it into  $\widehat{J}_{uu}, \widehat{J}_{uv}, \widehat{J}_{vu}, \widehat{J}_{vv}$  and compute  $\widehat{\mathcal{S}}$  and  $\widehat{\mathcal{N}}_0$ . Estimate the moment covariance  $\Sigma_L$  according to the sampling mechanism. For deterministic weights and independent samples with  $a_n = (\sum_i w_i^2)^{-1/2}$ , a plug-in estimator is

$$\widehat{\Sigma}_L = \frac{\sum_i w_i^2 \{\phi_L(x_i) - \widehat{m}_L\} \{\phi_L(x_i) - \widehat{m}_L\}^\top}{\sum_i w_i^2}.$$

For self-normalized importance weights with  $a_n = \sqrt{n}$ , use the influence estimate

$$\widehat{\Sigma}_L = \frac{1}{n} \sum_{i=1}^n (nw_i)^2 \{\phi_L(x_i) - \widehat{\mu}_{0,L}\} \{\phi_L(x_i) - \widehat{\mu}_{0,L}\}^\top,$$

where  $\widehat{\mu}_{0,L} = \mathbb{E}_{\widehat{\rho}_0} \phi_L(X)$ . This centering is specific to null calibration; intervals or standard errors away from the null should instead use the alternative-regime influence function or a bootstrap under the fitted alternative. The null  $p$ -value is then obtained by simulating

$$\sum_{j=1}^q \widehat{\omega}_j \chi_{1j}^2, \quad \widehat{\omega}_j = \text{eig}_j \left( \frac{1}{2} \widehat{\mathcal{S}}^{-1/2} \widehat{\mathcal{N}}_0 \widehat{\Sigma}_L \widehat{\mathcal{N}}_0^\top \widehat{\mathcal{S}}^{-1/2} \right), \quad (8)$$

against the observed  $a_n^2 \widehat{I}_L$ . In the correctly specified uniform-weight case this reduces to the ordinary  $\chi_q^2$  calibration for  $2n \widehat{I}_L$ .

## 6 THE SPHERE: FROM VMF TO HARMONIC STRUCTURE

We now return to the motivating case  $M = S^{d-1}$  with normalized surface measure  $\sigma$ , and make precise what a fitted concentration or entropy captures. A distribution on  $S^{d-1}$  can be non-uniform by preferring a direction, an axis, a great subsphere, or several separated modes. These have different implications for uncertainty, and the harmonic hierarchy separates them by matching increasingly rich angular moments.

### 6.1 Level 1: vMF as First-Order Uncertainty

Let  $\mathcal{V}_1$  be the span of linear coordinate functions  $x \mapsto a^\top x$ . Then

$$p_1(x) = \exp\{\eta^\top x - \psi_1(\eta)\},$$

which is the vMF distribution with natural parameter  $\eta = \kappa \mu$ ,  $\|\mu\| = 1$ . The empirical mean resultant vector is

$$\widehat{r} = \sum_{i=1}^n w_i x_i, \quad \widehat{R} = \|\widehat{r}\|.$$

The fitted direction is  $\widehat{\mu} = \widehat{r}/\widehat{R}$  when  $\widehat{R} > 0$ , and  $\widehat{\kappa}$  solves  $A_d(\widehat{\kappa}) = \widehat{R}$ , where  $A_d$  is the standard vMF mean-resultant function. The first entropy gap

$$\widehat{I}_1 = \widehat{D}_1$$

therefore measures the information explained by a nonzero mean direction. Reporting only  $\widehat{\kappa}$  is equivalent to reporting only the first level of the hierarchy.

This interpretation clarifies both the strength and the limitation of vMF uncertainty. When the distribution

is truly unimodal and roughly rotationally symmetric,  $\widehat{I}_1$  is the dominant term and vMF entropy is an appropriate uncertainty summary. When  $\widehat{I}_1$  is small, the correct conclusion is only that there is little first-order directional information. It does not imply that the distribution is close to uniform.

The local connection to the mean resultant length is explicit.

**Proposition 9** (Local form of the first-order gap). *If  $r(P) = \mathbb{E}_P[X]$  and  $\|r(P)\| \rightarrow 0$ , then*

$$I_1(P) = D_1(P) = \frac{d}{2} \|r(P)\|^2 + o\{\|r(P)\|^2\}.$$

### 6.2 Level 2: Fisher–Bingham-Type Structure

Let  $\mathcal{V}_2$  add traceless quadratic functions

$$x \mapsto x^\top Bx, \quad B = B^\top, \quad \text{tr}(B) = 0.$$

The level-2 density has the form

$$p_2(x) \propto \exp\{\eta^\top x + x^\top Bx\}.$$

This includes Fisher–Bingham and Bingham-type structure. The second gap

$$\widehat{I}_2 = \widehat{D}_2 - \widehat{D}_1$$

measures the additional information explained by second-order anisotropy.

This is the first level at which the method distinguishes directional uncertainty from axial uncertainty. For an antipodal mixture with equal mass near  $\mu$  and  $-\mu$ , the first moment cancels, but the matrix moment  $\mathbb{E}[XX^\top]$  has a dominant eigen-direction. For a girdle distribution concentrated around an equator, the leading eigen-direction is instead the normal to the low-density direction. Both phenomena are invisible to a vMF fit but visible through  $\widehat{I}_2$ .

The connection to the usual second-moment matrix is explicit. Let

$$Q(P) = \mathbb{E}_P[XX^\top], \quad Q_0 = I_d/d.$$

If the first moment is zero and  $Q(P) = Q_0$ , then the degree-2 moment constraint is uniform and  $I_2(P) = 0$  under the interior condition. Conversely, a nonzero traceless part of  $Q(P)$  forces a positive second-order gap. Near the uniform law, the gap has the following local form.

**Proposition 10** (Local form of the second-order gap). *If  $\mathbb{E}_P[X] = 0$  and  $\|Q(P) - Q_0\|_F \rightarrow 0$ , then*

$$I_2(P) = \frac{d(d+2)}{4} \|Q(P) - Q_0\|_F^2 + o\{\|Q(P) - Q_0\|_F^2\}.$$

Thus  $I_2$  is locally equivalent to squared Frobenius anisotropy, but with a global entropy interpretation. Appendix A.1 visualizes the two local approximations.

### 6.3 Higher Levels: Spherical Harmonic Exponential Families

Let  $\mathcal{H}_\ell$  be the spherical harmonic subspace of degree  $\ell$ , and take  $\mathcal{V}_L = \bigoplus_{\ell=1}^L \mathcal{H}_\ell$ . Then

$$p_L(x) = \exp \left\{ \sum_{\ell=1}^L \sum_{r=1}^{h_\ell} \lambda_{\ell r} Y_{\ell r}(x) - \psi_L(\lambda) \right\}.$$

Higher levels of  $L \geq 3$  answer a question that neither vMF nor Fisher–Bingham can settle: is the distribution structured because of a small number of separated angular modes? For example, three modes arranged symmetrically on  $S^1$  or four modes near tetrahedral directions on  $S^2$  can have weak first-order signal and limited second-order signal. The higher harmonic gaps are designed to reveal precisely this residual non-uniformity. Thus the hierarchy turns the vague statement “the fitted concentration is small” into a sharper statement about which harmonic orders carry information.

**Adequacy and regularization.** The gaps describe information explained by the chosen feature spaces; residual diagnostics and regularized fits are useful when a low-order model misses structure or an empirical moment lies near the boundary of the feasible moment body. Appendix B gives the maximum mean discrepancy (MMD)/Sobolev residuals and the regularized dual used in our reporting.

## 7 COMPUTATION

The level- $L$  fit solves the concave dual objective  $\ell_L(\lambda) = \lambda^\top \hat{m}_L - \psi_L(\lambda)$ , with gradient  $\hat{m}_L - \mathbb{E}_\lambda[\phi_L(X)]$  and Hessian  $-\text{Var}_\lambda\{\phi_L(X)\}$ . Level 1 uses standard vMF solvers, level 2 can use Fisher–Bingham/Bingham numerical methods and saddlepoint approximations for normalizing constants (Kume and Wood, 2005), and higher harmonic levels use quadrature, spherical Fourier transforms, or Monte Carlo. Score matching can initialize parameters, but entropy reporting requires the log-partition value  $\psi_L$ .

**Scalability in ambient dimension.** Exact full-harmonic fitting is primarily a low- and moderate-dimensional directional method. The full degree-2 increment on  $S^{d-1}$  adds

$$\dim\{\text{traceless quadratics}\} = d(d+1)/2 - 1$$

features, and the corresponding normalizing constant is difficult for large  $d$ . Therefore, for embedding-scale applications with  $d$  in the hundreds, the exact full  $L = 2$  model should not be used naively. Practical

high-dimensional variants should use structured feature spaces: low-rank quadratic features after projecting to an  $r$ -dimensional subspace, diagonal or block-diagonal quadratic terms, random sketches of harmonic features, or application-specific invariant features. In that case, the same definitions and KL-gap theory apply with  $\mathcal{V}_L$  replaced by the chosen structured subspace, but it should be interpreted as information explained by the chosen features, not full degree- $L$  spherical information. Exact rotation invariance from Theorem 3 survives only for deterministic invariant subspaces; a random sketch generally breaks exact invariance for a realized sketch, although it can be invariant in distribution if the sketching law is rotation-invariant. If a structured space  $\mathcal{V}_L^{\text{str}}$  is a subspace of the full harmonic space  $\mathcal{V}_L^{\text{full}}$  and the lower levels are shared, then monotonicity gives  $D_L^{\text{str}}(P) \leq D_L^{\text{full}}(P)$ . The difference is the information not retained by the structured features. In practice this loss can be probed by residual diagnostics such as (9) or by repeating the fit across several sketches or projections.

## 8 EXPERIMENTS

We evaluate whether the information gaps identify the kind of structure that makes vMF uncertainty adequate or misleading. We also compare the gaps with classical summaries such as  $\hat{R}$ ,  $\hat{\kappa}$ , and Frobenius second-moment anisotropy. All synthetic experiments and figures use fixed random seeds unless noted in the accompanying script. All reported gaps are in nats. The phrase “dominant gap” below refers to the largest point estimate. Formal significance near zero should be calibrated by Theorem 8, not by the alternative-regime delta method.

### 8.1 Controlled Experiments on the Circle

On the circle, the hierarchy is a Fourier maximum-entropy model with features

$$\phi_L(\theta) = \{\cos(k\theta), \sin(k\theta) : 1 \leq k \leq L\}.$$

We fit  $L = 1, 2, 3, 4$  by numerical quadrature on a grid of 4096 points. Each row in Table 1 averages 100 replicates with  $n = 400$  samples. Parentheses are Monte Carlo standard errors. “Pareto” weights are normalized independent Pareto weights, giving an effective sample size near 95.

The results match the intended interpretation. For a unimodal von Mises distribution, essentially all information is first-order. For an antipodal mixture,  $I_1$  is nearly zero while  $I_2$  is large, so a vMF entropy would falsely suggest high uncertainty. For a three-mode

Table 1: Fourier information gaps on  $S^1$ .

Scenario	Weights	ESS	$I_1$	$I_2$	$I_3$	$I_4$	$D_4$
vMF	uniform	400	1.028 (0.004)	0.003 (0.000)	0.002 (0.000)	0.004 (0.000)	1.037
vMF	Pareto	97	1.050 (0.010)	0.014 (0.002)	0.011 (0.002)	0.015 (0.003)	1.090
antipodal	uniform	400	0.003 (0.000)	0.722 (0.003)	0.003 (0.000)	0.009 (0.001)	0.736
antipodal	Pareto	94	0.017 (0.003)	0.757 (0.010)	0.011 (0.001)	0.018 (0.002)	0.803
trimodal	uniform	400	0.003 (0.000)	0.002 (0.000)	0.532 (0.003)	0.002 (0.000)	0.539
trimodal	Pareto	93	0.022 (0.005)	0.017 (0.003)	0.544 (0.009)	0.013 (0.002)	0.597

symmetric mixture,  $I_3$  carries the signal. Nonuniform weights reduce effective sample size and introduce small leakage into other gaps, but the dominant geometric component remains stable.

Appendix A.1 shows the fitted hierarchy for one trimodal replicate. Using the truncated harmonic residual (9) with  $a_\ell = 1$  and frequencies up to  $K_{\max} = 8$ , the same replicate gives  $R_1 = 0.421$ ,  $R_2 = 0.420$ , and  $R_3 = 0.083$ , so the residual drops when the relevant third harmonic is included.

## 8.2 Low-Order Experiments on the Two-Sphere

We next test the first two levels on the ordinary sphere. Level 1 uses linear features; level 2 adds traceless quadratic features. The log-partition function is approximated by Monte Carlo quadrature with 30,000 uniform points on  $S^2$ . Each row in Table 2 averages 30 replicates with  $n = 500$  and uniform weights.

Table 2: Low-order information gaps and classical summaries on  $S^2$ .  $A_Q = \|\sum_i w_i x_i x_i^T - I_3/3\|_F$ .

Scenario	$I_1$	$I_2$	$D_2$	$\hat{R}$	$\hat{\kappa}$	$A_Q$
vMF cloud	1.780 (0.006)	0.005 (0.001)	1.786	0.876	8.07	0.550
antipodal mixture	0.004 (0.001)	1.504 (0.008)	1.507	0.042	0.12	0.633
girdle distribution	0.003 (0.000)	0.919 (0.010)	0.922	0.041	0.12	0.363

These examples are the canonical failure modes for vMF concentration. The antipodal and girdle distributions have almost no mean direction, so  $\hat{R}$  and  $\hat{\kappa}$  suggest near-uniform first-order uncertainty. The second-order entropy gap identifies their strong axial or equatorial structure. The comparison with  $A_Q$  also shows why a raw second-moment norm is not a substitute for the decomposition: a concentrated vMF cloud has a large  $A_Q$  because first-order concentration induces anisotropic second moments, but its residual  $I_2$  is nearly zero after the mean-direction information has been explained.

## 8.3 Null Calibration on $S^2$

We also validate the second-order null calibration. The target distribution is uniform on  $S^2$ , and we test whether adding the five traceless quadratic features contributes information beyond the reduced model. Under uniform weights, Theorem 8 predicts  $W_n = 2n\hat{I}_2 \Rightarrow \chi_5^2$ . Under self-normalized importance

weights, samples are drawn from a vMF proposal with concentration 1.2 and reweighted back to the uniform target; here the ordinary  $\chi_5^2$  law is no longer calibrated, so we use the plug-in quadratic-form recipe in (8). Table 3 reports p-value quantiles; correct calibration should give approximately Uniform(0, 1) p-values.

Table 3: Finite-sample null calibration for  $I_2$  on  $S^2$  with  $n = 500$ . Uniform weights use 1000 replicates and importance weights use 400 replicates.

Sampling	calibration	ESS	$p_{.10}$	$p_{.50}$	$p_{.90}$	size .05	KS
equal	$\chi_5^2$	500	0.115	0.496	0.892	0.038	0.022
importance	naive $\chi_5^2$	317	0.013	0.256	0.770	0.215	0.252
importance	quadratic form	317	0.103	0.520	0.902	0.040	0.046

This experiment illustrates why the null theorem must be operationalized rather than replaced by a first-order standard error. With informative weights, the same point estimate  $\hat{I}_2$  requires a sandwich covariance and a quadratic-form tail calculation.

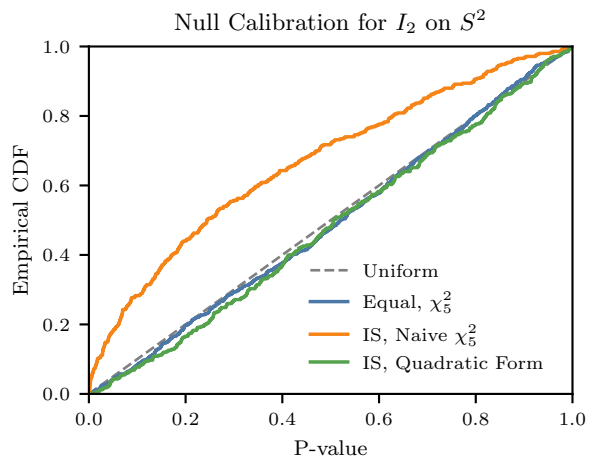


Figure 2: Empirical CDFs of null-calibration p-values for the three settings in Table 3.

A query-weighted digit illustration after projection to  $S^2$  is reported in Appendix A.2.

## 9 DISCUSSION

GID turns maximum-entropy fitting into an uncertainty profile for empirical measures on the sphere, interpreting a classical KL decomposition in a directional and operational way. In practice the gaps should be reported with residual diagnostics and effective sample size, and the significance of a new level assessed by the second-order calibration rather than an alternative-regime standard error, especially under informative weights. Principled selection of the harmonic order is left to future work.

---

## References

- Amari, S., Nagaoka, H., Amari, S., and Amari, S. (2007). *Methods of Information Geometry*. Number 191 in Translations of mathematical monographs. American Mathematical Society, Providence, Rhode Island.
- Amari, S.-I. (2001). Information geometry on hierarchy of probability distributions. *IEEE Transactions on Information Theory*, 47(5):1701–1711.
- Banerjee, A., Dhillon, I. S., Ghosh, J., and Sra, S. (2005). Clustering on the unit hypersphere using von mises-fisher distributions. *Journal of Machine Learning Research*, 6(46):1345–1382.
- Beran, R. (1979). Exponential Models for Directional Data. *The Annals of Statistics*, 7(6).
- Brown, L. D. (1986). *Fundamentals of Statistical Exponential Families with Applications in Statistical Decision Theory*. SPIE.
- Cohen, T. S. and Welling, M. (2015). Harmonic Exponential Families on Manifolds. In *Proceedings of the 32nd International Conference on Machine Learning - Volume 37, ICML’15*, pages 1757–1765, Lille, France. JMLR.org.
- Csiszar, I. (1975).  $\mathbb{I}$ -Divergence Geometry of Probability Distributions and Minimization Problems. *The Annals of Probability*, 3(1).
- Csiszar, I. and Matus, F. (2003). Information projections revisited. *IEEE Transactions on Information Theory*, 49(6):1474–1490.
- Fisher, R. (1953). Dispersion on a Sphere. *Proceedings of the Royal Society A: Mathematical, Physical and Engineering Sciences*, 217(1130):295–305.
- García-Portugués, E. and Verdebout, T. (2018). An overview of uniformity tests on the hypersphere.
- Jaynes, E. T. (1957). Information Theory and Statistical Mechanics. *Physical Review*, 106(4):620–630.
- Jupp, P. E. (2008). Data-driven Sobolev tests of uniformity on compact Riemannian manifolds. *The Annals of Statistics*, 36(3).
- Kent, J. T. (1982). The Fisher-Bingham Distribution on the Sphere. *Journal of the Royal Statistical Society Series B: Statistical Methodology*, 44(1):71–80.
- Kume, A. and Wood, A. T. A. (2005). Saddlepoint approximations for the Bingham and Fisher–Bingham normalising constants. *Biometrika*, 92(2):465–476.
- Mardia, K. V. and Jupp, P. E. (2000). *Directional statistics*. Wiley Series in Probability and Statistics. J. Wiley, Chichester; New York.
- Pedregosa, F., Varoquaux, G., Gramfort, A., Michel, V., Thirion, B., Grisel, O., Blondel, M., Prettenhofer, P., Weiss, R., Dubourg, V., Vanderplas, J., Passos, A., Cournapeau, D., Brucher, M., Perrot, M., and Duchesnay, É. (2011). Scikit-learn: Machine Learning in Python. *Journal of Machine Learning Research*, 12(85):2825–2830.
- Self, S. G. and Liang, K.-Y. (1987). Asymptotic Properties of Maximum Likelihood Estimators and Likelihood Ratio Tests under Nonstandard Conditions. *Journal of the American Statistical Association*, 82(398):605–610.

## A SUPPLEMENTARY EXPERIMENTS AND FIGURES

### A.1 Additional Diagnostics and Figures

The following two figures support the main experiments without being necessary for the central narrative. They are included here with enough detail to make each example reproducible and interpretable without referring back to the main text.

**Trimodal circle hierarchy.** The first diagnostic uses one replicate from the trimodal  $S^1$  experiment. We draw  $n = 500$  angles from the equally weighted mixture

$$\frac{1}{3} \sum_{j=0}^2 \text{vM}\{2\pi j/3, 5.5\},$$

where  $\text{vM}(\mu, \kappa)$  denotes the von Mises distribution on the circle with mean angle  $\mu$  and concentration  $\kappa$ . All sample weights are uniform in this display. We fit the Fourier maximum-entropy hierarchy with features

$$\{\cos(k\theta), \sin(k\theta) : 1 \leq k \leq L\}, \quad L = 1, 2, 3,$$

using numerical quadrature on a grid of 4096 angles. For visualization only, the empirical curve is a von Mises kernel density estimate with kernel concentration 14. Figure 3 shows that the first- and second-order projections are nearly unable to represent the threefold symmetry, while the  $L = 3$  projection fills in the three modes. This is the qualitative mechanism behind the dominant  $I_3$  gap reported for the trimodal rows of Table 1.

**Population local-form validation on  $S^2$ .** The second diagnostic checks the two local interpretations in Section 6. This is a numerical population calculation rather than a finite-sample experiment. For the first-order panel, we use the exact vMF family on  $S^2$  with concentration values  $\kappa \in [0.02, 1.5]$ . For each  $\kappa$ , we compute the exact entropy deficit

$$I_1(\kappa) = \kappa A_3(\kappa) - \log\{\sinh(\kappa)/\kappa\}$$

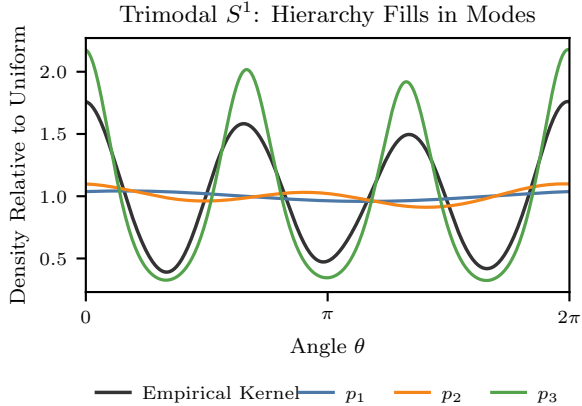


Figure 3: Trimodal circle example. The empirical kernel density has three modes;  $p_1$  and  $p_2$  miss the structure, while  $p_3$  captures it, matching the dominant  $I_3$  gap in Table 1.

with respect to normalized uniform surface measure and compare it with the local approximation  $(d/2)\|r\|^2$  for  $d = 3$  and  $\|r\| = A_3(\kappa)$ . For the second-order panel, we use the antipodally symmetric Bingham path  $p_t(x) \propto \exp\{tx^\top B_0 x\}$  for  $B_0 = \text{diag}(1, -1/2, -1/2)$  and  $t \in [0.02, 1.2]$ . The normalizing constant, second moment  $Q_t$ , and entropy deficit are approximated by a deterministic Fibonacci quadrature rule with 80,000 points on  $S^2$ . We then compare the computed second-order deficit with the local proxy  $(d(d+2)/4)\|Q_t - I_d/d\|_F^2$ . Figure 4 shows that both proxies agree with the corresponding information gaps near the uniform distribution, as predicted by the local expansions.

## A.2 Additional Real-Data Table

We use the handwritten digits dataset distributed with scikit-learn (Pedregosa et al., 2011). The 64-dimensional images are standardized, projected to three principal components, and normalized to  $S^2$ . For a query digit, weights over all examples are assigned by a softmax of cosine similarity in the original standardized image space with temperature  $\tau = 6$ , and the level-1 and level-2 models are fit to the query-specific empirical measure. This is a projected spherical workflow, not full embedding-scale harmonic fitting.

The query “0” produces a concentrated directional neighborhood with additional second-order anisotropy. The query “8” is more diffuse after projection, with much smaller cumulative information and lower effective sample size.

Table 4: Query-weighted digit embeddings after projection to  $S^2$ . Class mass lists the three largest label masses induced by the query weights.

Query	ESS	$I_1$	$I_2$	$D_2$	class mass
0	162.6	1.693	0.271	1.963	0:0.85, 9:0.05, 4:0.03
1	138.2	1.177	0.158	1.335	1:0.72, 8:0.06, 4:0.06
8	85.5	0.247	0.034	0.281	8:0.46, 3:0.12, 9:0.11

## B DIAGNOSTICS, REPORTING, AND REGULARIZATION

### B.1 Model Adequacy and Residual Diagnostics

The entropy gaps describe information explained by the chosen feature hierarchy. They do not by themselves prove that level  $L$  is adequate. A low-order model can have high fitted entropy either because the distribution is genuinely diffuse or because the features miss the relevant structure. We therefore recommend reporting a residual diagnostic together with the gaps.

One option is an MMD residual. Let  $k$  be a positive definite kernel on  $M$  and define

$$R_L^2(\hat{P}_w) = \text{MMD}_k^2(\hat{P}_w, \hat{p}_L \nu).$$

On the sphere, a Sobolev or harmonic residual is also natural:

$$R_L^2(\hat{P}_w) = \sum_{\ell > L} a_\ell \sum_{r=1}^{h_\ell} \left| \sum_i w_i Y_{\ell r}(x_i) - \int Y_{\ell r} \hat{p}_L d\sigma \right|^2. \quad (9)$$

Here  $a_\ell \geq 0$  are user-chosen Sobolev weights, for example  $a_\ell = \{1 + \ell(\ell + d - 2)\}^s$  for order  $s$ , or simply  $a_\ell \equiv 1$  for an unweighted truncated diagnostic. If  $R_L$  is large, then  $U_L$  should not be interpreted as a complete uncertainty summary.

### B.2 Reporting Details

For future applications, we recommend reporting: (i) entropy gaps  $\hat{I}_\ell$ ; (ii) cumulative effective uncertainty  $\hat{U}_L$ ; (iii) residual diagnostics  $R_L$ ; (iv) the effective sample size  $1/\sum_i w_i^2$ ; (v) the feature spaces used, including any projection or sketch; (vi) optimization tolerances, quadrature size, random seeds, and regularization strength; and (vii) null calibration by Theorem 8 or a null-respecting bootstrap when formal level selection is performed. A simple pre-specified selection rule is to compute level-wise p-values from (8), apply Holm correction over  $L = 1, \dots, L_{\max}$ , and choose the smallest level after which no later gap is significant and the residual diagnostic is below a user-specified tolerance. We use descriptive gaps in the present experiments; optimal order selection is left as a separate problem.

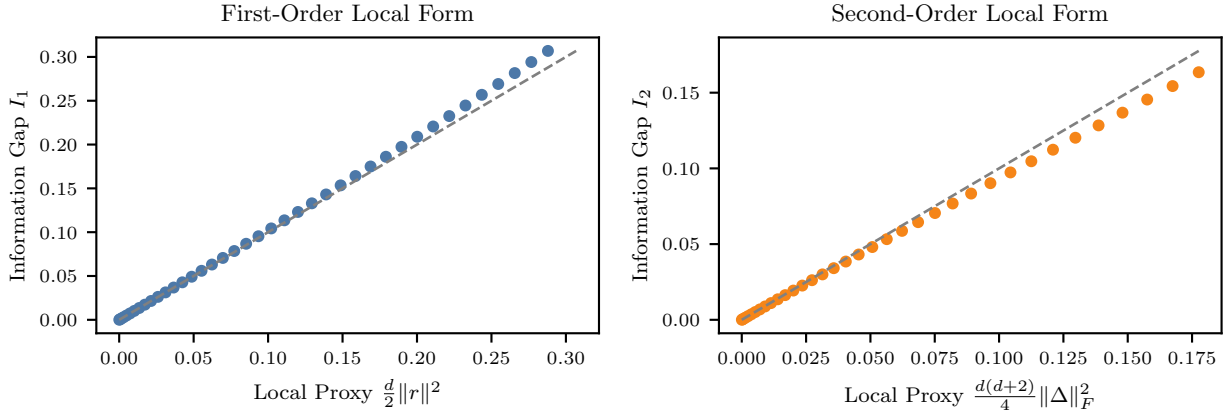


Figure 4: Numerical validation of the local interpretations on  $S^2$ . Left: the first gap agrees with  $\frac{d}{2}\|r\|^2$  near uniformity. Right: the second gap agrees with  $\frac{d(d+2)}{4}\|Q - I_d/d\|_F^2$  near uniformity. Dashed lines are identities.

### B.3 Boundary and Regularization

If  $\hat{m}_L \in \partial\mathcal{M}_L$ , then no finite natural parameter may solve  $\nabla\psi_L(\lambda) = \hat{m}_L$ . Geometrically, the empirical moment vector can be explained only by a distribution supported on a face of the moment body. This is the same phenomenon that produces nonexistence of MLEs in other exponential families.

A regularized dual objective

$$\lambda^\top \hat{m}_L - \psi_L(\lambda) - \rho(\lambda)$$

is strictly concave when  $\rho$  is strongly convex. Its solution always exists under mild coercivity conditions. For ridge regularization  $\rho(\lambda) = \alpha\|\lambda\|^2/2$ , the first-order condition becomes

$$\nabla\psi_L(\lambda) + \alpha\lambda = \hat{m}_L.$$

Thus the fitted model approximately, rather than exactly, matches the empirical moments. As  $\alpha \downarrow 0$ , the regularized solution approaches the unregularized solution when the latter exists; if the unregularized solution does not exist, the norm  $\|\lambda_\alpha\|$  typically diverges, providing a diagnostic for boundary behavior.

## C PROOFS

### C.1 Existence of the Maximum-Entropy Projection

We recall the standard finite-dimensional exponential-family argument. Let  $\phi : M \rightarrow \mathbb{R}^m$  be continuous and let

$$\mathcal{M} = \text{conv}\{\phi(x) : x \in M\}.$$

Since  $M$  is compact and  $\phi$  is continuous,  $\mathcal{M}$  is compact. Define

$$\psi(\lambda) = \log \int_M \exp\{\lambda^\top \phi(x)\} d\nu(x).$$

The gradient and Hessian are

$$\begin{aligned} \nabla\psi(\lambda) &= \mathbb{E}_\lambda[\phi(X)], \\ \nabla^2\psi(\lambda) &= \text{Var}_\lambda\{\phi(X)\}. \end{aligned}$$

After quotienting out directions  $a$  for which  $a^\top \phi(x)$  is constant  $\nu$ -almost surely, the Hessian is positive definite. Hence  $\psi$  is strictly convex on the minimal natural parameter space. Because  $M$  is compact and  $\phi$  is continuous,  $\psi$  is finite on all of the minimal natural parameter space and the family is regular and steep in the standard finite-dimensional sense (Brown, 1986). Standard exponential-family theory implies that the mean map  $\nabla\psi$  maps the natural parameter space diffeomorphically onto  $\text{ri}(\mathcal{M})$ . Therefore, for every  $m \in \text{ri}(\mathcal{M})$ , there is a unique natural parameter  $\lambda(m)$  satisfying  $\nabla\psi(\lambda(m)) = m$ .

The density

$$p_m(x) = \exp\{\lambda(m)^\top \phi(x) - \psi(\lambda(m))\}$$

is feasible. For any feasible density  $q$ ,

$$\begin{aligned} \text{KL}(q\nu \| p_m\nu) &= \int q \log q d\nu - \int q \log p_m d\nu \\ &= \int q \log q d\nu - \lambda(m)^\top m + \psi(\lambda(m)). \end{aligned}$$

Since the last two terms are fixed over the constraint set, minimizing  $\int q \log q d\nu$  is equivalent to minimizing  $\text{KL}(q\|p_m)$ . The unique minimizer is  $q = p_m$ . Equivalently,  $p_m$  uniquely maximizes entropy over the moment constraint set.

## C.2 Proof of Theorem 1

Because the feature spaces are nested, the level- $L$  constraint set is contained in the level- $(L-1)$  constraint set. Maximizing entropy over a smaller set cannot yield a larger entropy. Since  $D_L = -h(p_L^P)$ , this gives monotonicity:

$$D_0(P) \leq D_1(P) \leq \dots \leq D_L(P).$$

To prove the KL-gap identity, write the level- $(L-1)$  density as

$$\log p_{L-1}^P(x) = \lambda_{L-1}^\top \phi_{L-1}(x) - \psi_{L-1}(\lambda_{L-1}).$$

Since the level- $L$  constraints include the level- $(L-1)$  constraints,  $p_L^P$  and  $p_{L-1}^P$  have the same moments against  $\phi_{L-1}$ :

$$\int \phi_{L-1} p_L^P d\nu = \int \phi_{L-1} p_{L-1}^P d\nu = m_{L-1}(P).$$

Therefore

$$\begin{aligned} \int p_L^P \log p_{L-1}^P d\nu &= \lambda_{L-1}^\top m_{L-1}(P) - \psi_{L-1}(\lambda_{L-1}) \\ &= \int p_{L-1}^P \log p_{L-1}^P d\nu. \end{aligned}$$

It follows that

$$\begin{aligned} \text{KL}(p_L^P \nu \parallel p_{L-1}^P \nu) &= \int p_L^P \log p_L^P d\nu - \int p_L^P \log p_{L-1}^P d\nu \\ &= D_L(P) - D_{L-1}(P). \end{aligned}$$

This proves the identity. Summing over  $\ell$  yields (4).

## C.3 Proof of Theorem 2

Let  $\tilde{\phi} = T\phi$ , with  $T$  invertible. The constraint

$$\int \tilde{\phi} p d\nu = \int \tilde{\phi} dP$$

becomes

$$T \int \phi p d\nu = T \int \phi dP,$$

which is equivalent to the original constraint. Thus the feasible set in the primal maximum-entropy problem is unchanged. Therefore the maximizer  $p_L^P$  and all entropy-based quantities are unchanged.

## C.4 Proof of Theorem 3

Let  $g$  be an isometry. Since  $g$  preserves normalized Riemannian volume, the map  $p \mapsto p \circ g^{-1}$  is an entropy-preserving bijection between densities. If  $\mathcal{V}_L$  is invariant under the group action, then matching

all moments in  $\mathcal{V}_L$  under  $P$  is equivalent, after pushforward, to matching all moments in  $\mathcal{V}_L$  under  $g\#P$ . Hence the maximum-entropy projection for  $g\#P$  is the pushforward of the maximum-entropy projection for  $P$ :

$$p_L^{g\#P} = g\#p_L^P.$$

KL divergence to  $\nu$  is invariant under measure-preserving transformations, so  $D_L(g\#P) = D_L(P)$ . The statements for  $U_L$  and  $I_L$  follow immediately.

## C.5 Proof of Theorem 6

Under Assumption 4, the mean map  $m \mapsto \lambda_L(m)$  is continuous in a neighborhood of  $m_L(P)$ . Since  $m_L(P) \in \text{ri}(\mathcal{M}_L)$  and  $\hat{m}_L \rightarrow m_L(P)$  in probability, the event  $\{\hat{m}_L \in \text{ri}(\mathcal{M}_L)\}$  has probability tending to one; all plug-in quantities are considered on this event. Assumption 5 gives  $\hat{m}_L \rightarrow m_L(P)$  in probability. The continuous mapping theorem implies

$$\hat{\lambda}_L = \lambda_L(\hat{m}_L) \xrightarrow{P} \lambda_L(m_L(P)).$$

The entropy deficit can be written as the Legendre transform

$$D_L(m) = \lambda_L(m)^\top m - \psi_L(\lambda_L(m)),$$

which is continuous on the relative interior of the moment body. Therefore  $\hat{D}_L \rightarrow D_L(P)$  in probability. Since  $\hat{I}_L = \hat{D}_L - \hat{D}_{L-1}$ , the increment consistency follows.

## C.6 Proof of Theorem 7

The entropy deficit  $D_L(m)$  is the convex conjugate of  $\psi_L$  restricted to the feasible moment body. On the relative interior, it is differentiable and

$$\nabla_m D_L(m) = \lambda_L(m).$$

Applying the delta method to the moment CLT gives

$$a_n(\hat{D}_L - D_L) \Rightarrow N(0, \lambda_L^\top \Sigma_L \lambda_L).$$

For the increment, view  $D_{L-1}$  as a function of the level- $L$  moment vector through the projection  $\Pi_{L-1} m_L$ . Its gradient in level- $L$  coordinates is  $\Pi_{L-1}^\top \lambda_{L-1}$ . Therefore the gradient of  $I_L = D_L - D_{L-1}$  is

$$\gamma_L = \lambda_L - \Pi_{L-1}^\top \lambda_{L-1}.$$

A second application of the delta method proves (6).

## C.7 Proof of Proposition 9

Under the uniform law on  $S^{d-1}$ ,  $\mathbb{E}[X] = 0$  and  $\text{Var}(X) = I_d/d$ . The level-1 exponential tilt is  $p_1(x) \propto \exp(\eta^\top x)$ . For small  $\eta$ ,

$$r(P) = \mathbb{E}_\eta[X] = \frac{\eta}{d} + o(\|\eta\|).$$

The entropy deficit has the local Fisher expansion

$$D_1 = \frac{1}{2} \eta^\top \text{Var}_0(X) \eta + o(\|\eta\|^2) = \frac{\|\eta\|^2}{2d} + o(\|\eta\|^2).$$

Substituting  $\eta = dr(P) + o(\|r(P)\|)$  gives

$$I_1(P) = D_1(P) = \frac{d}{2} \|r(P)\|^2 + o\{\|r(P)\|^2\}.$$

### C.8 Proof of Proposition 10

For  $X$  uniform on  $S^{d-1}$ ,

$$\mathbb{E}[X_i X_j X_k X_l] = \frac{\delta_{ij} \delta_{kl} + \delta_{ik} \delta_{jl} + \delta_{il} \delta_{jk}}{d(d+2)}.$$

For a traceless symmetric matrix  $B$ , this gives

$$\begin{aligned} \mathbb{E}\{(X^\top B X) X X^\top\} &= \frac{2B}{d(d+2)}, \\ \mathbb{E}\{(X^\top B X)^2\} &= \frac{2\text{tr}(B^2)}{d(d+2)}. \end{aligned}$$

Near the uniform law, the degree-2 natural parameter  $B$  and the traceless second moment  $\Delta = Q(P) - I_d/d$  satisfy

$$\Delta = \frac{2B}{d(d+2)} + o(\|B\|_F).$$

The entropy deficit of the corresponding quadratic exponential tilt is

$$D_2 = \frac{1}{2} \mathbb{E}\{(X^\top B X)^2\} + o(\|B\|_F^2) = \frac{\text{tr}(B^2)}{d(d+2)} + o(\|B\|_F^2).$$

Since the first moment is zero,  $D_1 = 0$  and  $I_2 = D_2$ . Substituting  $B = \frac{d(d+2)}{2} \Delta + o(\|\Delta\|_F)$  yields

$$I_2(P) = \frac{d(d+2)}{4} \|\Delta\|_F^2 + o(\|\Delta\|_F^2),$$

as claimed.

### C.9 Proof of Theorem 8

Write  $m = (m_u, m_v)$  for the level- $L$  moment vector. At the null  $I_L(P) = 0$ , the full and reduced projections coincide and have natural parameter  $\theta_0 = (\alpha_0, 0)$ . Let

$$\mathcal{J}_0 = \nabla^2 \psi_L(\theta_0) = \begin{pmatrix} J_{uu} & J_{uv} \\ J_{vu} & J_{vv} \end{pmatrix}.$$

Minimality implies  $\mathcal{J}_0 \succ 0$ , hence  $J_{uu} \succ 0$  and the Schur complement  $\mathcal{S} = J_{vv} - J_{vu} J_{uu}^{-1} J_{uv}$  is positive definite. The Hessian of the Legendre transform  $D_L(m)$  at the null is  $\mathcal{J}_0^{-1}$ . The reduced deficit  $D_{L-1}(m_u)$  has Hessian  $J_{uu}^{-1}$  in the  $u$  coordinates. Therefore

the Hessian of the gap  $I_L(m_u, m_v) = D_L(m_u, m_v) - D_{L-1}(m_u)$  is

$$\mathcal{J}_0^{-1} - \begin{pmatrix} J_{uu}^{-1} & 0 \\ 0 & 0 \end{pmatrix}.$$

Using the block inverse formula, this difference equals

$$\mathcal{N}_0^\top \mathcal{S}^{-1} \mathcal{N}_0, \quad \mathcal{N}_0 = \begin{pmatrix} -J_{vu} J_{uu}^{-1} & I_q \end{pmatrix}.$$

Since  $I_L(P) = 0$  and  $\nabla I_L = 0$  at the null, the second-order Taylor expansion gives

$$\widehat{I}_L = \frac{1}{2} (\widehat{m}_L - m_L)^\top \mathcal{N}_0^\top \mathcal{S}^{-1} \mathcal{N}_0 (\widehat{m}_L - m_L) + o_p(a_n^{-2}).$$

Multiplying by  $a_n^2$  and applying the moment CLT proves (7). If the sample is correctly specified i.i.d. from the reduced model, then  $\Sigma_L = \mathcal{J}_0$ , so  $\mathcal{N}_0 \Sigma_L \mathcal{N}_0^\top = \mathcal{S}$  and  $2a_n^2 \widehat{I}_L \Rightarrow \chi_q^2$ .

### C.10 CLT for Independent Samples with Deterministic Weights

Suppose  $X_i \stackrel{\text{i.i.d.}}{\sim} P$ , weights are deterministic, and  $\sum_i w_i = 1$ . Let  $Z_i = \phi_L(X_i) - m_L(P)$ . Then

$$\widehat{m}_L - m_L(P) = \sum_i w_i Z_i.$$

If  $\mathbb{E} \|Z_i\|^2 < \infty$  and the Lindeberg condition

$$\frac{\max_i w_i}{(\sum_j w_j^2)^{1/2}} \rightarrow 0$$

holds, then

$$\frac{\widehat{m}_L - m_L(P)}{(\sum_i w_i^2)^{1/2}} \Rightarrow N(0, \text{Var}_P\{\phi_L(X)\}).$$

Because  $M$  is compact and  $\phi_L$  is continuous, the moment condition is automatic. This identifies  $a_n = (\sum_i w_i^2)^{-1/2}$  and shows how the usual effective sample size enters the uncertainty of the estimated entropy gaps.